A testosterone metabolite 19-hydroxyandrostenedione induces neuroendocrine trans-differentiation of prostate cancer cells via an ectopic olfactory receptor

Tatjana Abaffy[1*], James R. Bain[2], Michael J. Muehlbauer[2], Ivan Spasojevic[3], Shweta Lodha[1], Elisa Bruguera[1], Sara K. O'Neal[2], So Young Kim[1], Hiroaki Matsunami[1]

[1]Department of Molecular Genetics and Microbiology

[2]Duke Molecular Physiology Institute

[3]Duke Cancer Institute

*Corresponding author and lead contact

Abstract

Olfactory receptor OR51E2, also known as a Prostate Specific G-Protein Receptor, is highly expressed in prostate cancer but its function is not well understood. Through *in silico* and *in vitro* analyses, we identified 24 agonists and 1 antagonist for this receptor. We detected that agonist 19-hydroxyandrostenedione, a product of the aromatase reaction, is endogenously produced upon receptor activation. We characterized the effects of receptor activation on metabolism using a prostate cancer cell line and demonstrated decreased intracellular anabolic signals and cell viability, induction of cell cycle arrest, and increased expression of neuronal markers. Furthermore, upregulation of neuron-specific enolase by agonist treatment was abolished in OR51E2-KO cells. The results of our study suggest that OR51E2 activation results in neuroendocrine trans-differentiation. These findings reveal a new role for OR51E2 and establish this G-protein coupled receptor as a novel therapeutic target in the treatment of prostate cancer.

Keywords:

Olfactory receptor, PSGR, prostate cancer, neuroendocrine trans-differentiation, neuron-specific enolase, agonists, 19-hydroxyandrostenedione, metabolites, estrogen, CRISPR/Cas9, CRPC, serine, threonine, phosphoenolpyruvate, glutamine, metabolomics

Significance:

Prostate cancer is the second most common cancer in men. Most deaths from prostate cancer are due to the progression of localized disease into metastatic, castration-resistant prostate cancer characterized by increased number of neuroendocrine-like cells. These neuroendocrine-like cells are non-proliferating, terminally differentiated cells. Olfactory receptor OR51E2, also known as a Prostate Specific G-Protein Receptor, is highly expressed in prostate cancer, and its expression correlates with disease progression. Here, we identify and validate novel endogenous ligands for this receptor. We show that activation of OR51E2 by newly-discovered prostate cancer-relevant agonists facilitates cellular transformation, resulting in neuroendocrine trans-differentiation, a characteristic phenotype of castrate resistant prostate cancer. Our results establish this G-protein coupled receptor as a novel and therapeutic target for castration-resistant prostate cancer.

Highlights:

- Discovery of novel agonists for olfactory receptor OR51E2/PSGR highly relevant to prostate cancer pathology
- Activation of OR51E2 receptor by agonist *N*-acetyl-*N*-formyl-5-methoxykynurenamine (AFMK) results in release of 19-hydroxyandrostenedione (19-OH AD) from the prostate cancer cells indicating its endogenous production
- Activation of OR51E2 receptor by 19-OH AD, AFMK, and propionic acid decreases anabolic and proliferative signals

- Activation of OR51E2 receptor by 19-OH AD and AFMK increases markers specific for neuroendocrine trans-differentiation (NEtD)
- Ablation of the OR51E2 gene in prostate cancer cells treated with agonist 19-OH AD significantly reduces neuron-specific enolase

INTRODUCTION

G-protein coupled receptors (GPCRs) have emerged as important factors in tumor growth and metastasis [1-3]. Several GPCRs, such as the 5HT1c serotonin receptor [4], the M1, M3, and M5 muscarinic receptors [5], and the α1B-ADR adrenergic receptor [6], can function as oncogenes when persistently activated. These GPCRs, which are normally expressed in fully differentiated, post-mitotic neuronal cells, are able to induce cellular oncogenic transformation when introduced to an ectopic environment of proliferating cells and activated by agonist [7,8]. In addition to oncogenes and tumor-suppressor genes essential for cancer initiation and progression, autocrine and/or paracrine secretion of GPCR-activating molecules and their downstream signaling events affect tumor growth, survival, and metastasis [1,9-14].

Olfactory receptors (ORs) are the largest family of GPCRs present in the olfactory epithelium but are also found in various ectopic or non-olfactory locations such as prostate, heart, placenta, embryo, erythroid cells, spleen, kidney, gut, tongue, and carotid body [15-17]. Some ectopic ORs also play roles in chemotaxis [18], muscle regeneration [19], blood pressure regulation [20], and hypoxia response [21]. OR51E2, or Prostate Specific G-protein Receptor (PSGR), is one of the most highly conserved and broadly expressed ectopic ORs [22-24]. OR51E2 is present in healthy prostate tissue and shows significantly increased expression in prostate intraepithelial neoplasia (PIN), prostate adenocarcinoma (PC), and castration-resistant prostate cancer (CRPC) [25-32].

What is the role of OR51E2 in prostate cancer?

The majority of prostate tumors start as androgen-dependent adenocarcinomas. As localized cancer progresses to a metastatic state, the number of neuroendocrine (NE)-like cells increases, contributing to the development of a highly aggressive form of castrate-resistant prostate cancer (CRPC) known as neuroendocrine prostate cancer (NEPC) [33,34]. Many clinical studies have demonstrated a correlation between neuroendocrine trans-differentiation (NEtD) and PC progression with poor prognosis [35]. Tumor-derived NE-like cells are localized in tumor foci and are non-proliferating, terminally differentiated cells rich in serotonin and positive for NE markers, including neuron-specific enolase (NSE) and chromogranin A (CGA) [35].

The molecular mechanism underlying development of a neuroendocrine phenotype in PC is not fully understood. In the androgen-dependent PC cell line LNCaP, serum deprivation and agents that increase cAMP also increase expression of NEtD markers and genes indicative of neuronal phenotype [36].

In the olfactory system, ORs signal via the canonical cAMP pathway [37], and several reports have indicated cAMP-mediated signaling for ectopic ORs [38-40]. Furthermore, high expression of the OR downstream targets adenylate cyclase 3 and Gαolf was recently identified in prostate tissue, supporting the role of a cAMP-mediated pathway in ectopic OR activation [22,41]. We hypothesized that agonist-mediated activation of OR51E2 increases cAMP and facilitates cellular transformation, resulting in NEtD. Thus, ectopic expression of this GPCR in proliferating cells and ligand-dependent activation could enable this receptor to function as an oncogene.

Recently, it has been demonstrated that overexpression of OR51E2/PSGR in a PSGR-Pten (Δ/Δ) mouse model accelerates PC development and progression [42]. Furthermore, β-ionone, an agonist for OR51E2, decreased proliferation and increased invasiveness of human PC cells [43-45].

In this paper, we aimed to identify biologically relevant OR51E2 ligands using a combination of *in silico* investigations and experimental validation, and we also set out to study the effects of these ligands on androgen-dependent LNCaP cells. Currently identified OR51E2 agonists include the short-chain fatty acids acetate and propionate [20,46], steroid derivatives, β-ionone [43], and lactate [21]. However, it is not known whether activation of OE51E2 by endogenous ligands is involved in PC pathogenesis.

Here, we virtually screened >2,500 metabolites, experimentally validated 55 of these candidates *in vitro*, and ultimately identified 24 new agonists and 1 antagonist for the human OR51E2 receptor. Among the agonists, we identified 19-hydroxyandrostenedione (19-OH AD)—which is synthesized by aromatase, an enzyme highly expressed in NEPC and CRPC—and *N*-acetyl-*N*-formyl-5-methoxykynurenamine (AFMK), a tryptophan and melatonin metabolite. We detected endogenous production of 19-OH AD in the LNCaP cells stimulated with AFMK agonist. The identity of the newly discovered agonists, as well as significant differences in metabolomics signatures in agonist-stimulated PC cells indicative of non-proliferation, prompted us to further investigate their effects on cell viability, cell cycle status, and several NE markers to examine if OR51E2 receptor activation drives NEtD.

RESULTS

In Vitro Validation of Ligands Predicted *in Silico*

A structural model of OR51E2 was made *in silico* using Modeller (see Materials and Methods for details). To experimentally validate our virtual library screening (VLS) predictions, we used an *in vitro* heterologous expression system [47] in which Hana 3A cells transfected with the OR51E2 receptor were stimulated with the top candidate ligands. Responses were subsequently measured with a

cAMP-mediated luciferase reporter gene assay. First, a small library of 33 compounds identified as PC-associated metabolites was selected from the Human Metabolome Database HMDB [48]. These compounds were identified from previous reports [49-51]. Additional compounds previously identified as OR51E2 agonists were also included: 1,4,6-androstatriene-17-β-ol-3-one, 1,4,6-androstatriene-3,17-dione, 6-dehydrotestosterone, and β-ionone [43]. Thus, a total of 37 compounds were used for the initial, small-scale VLS (**Table S4**). Two scoring functions, Score and mfScore, were used to predict the best binders. The top 9 compounds from each score list (italicized in **Table S4)** were then tested *in vitro,* and the following metabolites were identified as novel agonists for OR51E2 (bold and italics): bradykinin, kojibiose, glycylglycine, L-histidinol N-acetylglutamic acid, and D-alanyl-D-alanine. We also confirmed the previously reported agonist 1,4,6-androstatriene-3,17-dione (**Figure S2**) [43].

Next, a larger library of 2,511 human metabolites from the HMDB was selected for virtual screening and docking into the receptor pocket (**Figures 1A and 1B**). Here, the top potential ligands (in italics, **Tables S1 and S2)** were tested *in vitro* using a biologically relevant concentration range reported in the HMDB, and concentration-response curves were subsequently produced**.** In total, 55 compounds were tested (9 and 46, from the smaller and larger screens, respectively), and 24 agonists (**Figures 1C, and S2 and S3)** and 1 antagonist for OR51E2 (**Figure 1C**) were identified. In each experiment, OR51E2-expressing Hana3A cells were also stimulated with a known agonist, 1 mM propionic acid (PA), so we were able to compare the efficacy of each metabolite relative to PA. Furthermore, potency values (EC_{50}) were determined (**Table 1)**. Glycylglycine was the most efficient agonist, while L- histidinol was the most potent. Diverse metabolites were discovered as novel agonists for OR51E2. Concentration-response curves for metabolites from the large VLS screen that did not activate the receptor are presented in **Figure S4**.

Some of the newly discovered agonists are: 19-hydroxyandrostenedione (19-OH AD), a hypertensive steroid (vasopressor) secreted by the adrenal gland [52-54], an intermediate in estrogen synthesis from testosterone [55] also found in porcine testes [56] and rat ovarian granulosa cells [57]; acetyl-N-formyl-5-methoxykynurenamine (AFMK), a melatonin and kynurenamine metabolite previously reported to be abundant in aggressive PC [58]; estradiol [59]; adenosine-2,3-cyclic phosphate, a positional isomer of the second messenger 3',5'-cAMP [60]; 8-hydroxyguanine, a marker of DNA damage; α-ketoglutaric acid, an intermediate in the citric acid cycle; urea; glycine; and palmitic acid.

Because *in situ* estrogen production is an important factor in prostate carcinogenesis, and since the expression of aromatase, the enzyme that synthetizes estrogens from androgens, is increased 30-fold in PC, we decided to further examine the presence and production of 19-OH AD in LNCaP cells [61,62].

Endogenous 19-OH AD production upon OR51E2 activation with AFMK

We have developed a liquid chromatography/mass spectrometry (LC-MS/MS) assay for the measurements of 19-OH AD in the cell media. LNCaP cells were stimulated with newly discovered agonist, 250 µM AFMK, for 3 days, and the 19-OH AD was measured in the cell medium (**Figure 2**). We used CD-phenol free RPMI1640 medium (**Figure 2A**) and regular RPMI1640 medium (**Figure 2B**) to estimate production of 19-OH AD. Three times more 19-OH AD was detected when cells were stimulated in CD-phenol free medium (0.83 *vs.* 0.27ng/mL). No 19-OH AD was detected in unstimulated cells (dotted lines in **Figures 2A and 2B**).

Metabolomic Signatures of LNCaP Cells Treated with Selected OR51E2 Agonists

In addition to the newly discovered agonists 19-OH AD and AFMK, we also selected the previously identified OR51E2 agonist propionic acid (PA) for metabolomics analysis [46]. Cells were incubated with 100 nM 19-OH AD, 250 µM AFMK, and 1 mM PA for 72 h, and non-targeted metabolomics

analysis was performed to identify metabolites that differed significantly in the cell lysate and conditioned medium (CM). Agonist treatment resulted in pronounced intra- and extra- cellular changes in metabolomic signatures, as seen in heat maps (**Figures S5 and S6,** respectively). Differentially expressed features/metabolites identified in each group using the t-test ($P < 0.05$) and fold change (2-fold or greater) are presented in **Figures S5-S10** and **Tables S5-S10.**

The top 15 differentially expressed extracellular metabolites are presented in **Figures 3A, 3B, and 3C**. All 3 agonists also produced robust intracellular decreases in amino acids, especially serine and threonine, and also 2 glycolytic intermediates: glucose-6-P and fructose-6-P (**Figure 3D, 3E and 3F**). Furthermore, agonist treatment resulted in decreases in both methionine and glycine levels. In addition to decreased lactic acid, significant decreases were noted in fumaric, malic, and succinic acids, all intermediates of the TCA. Interestingly, we detected an increased level of phosphoenolpyruvate (PEP) in all agonist-treated samples (fold change analysis, **Figures S7B, S8B and S9B**). We also observed decreased levels of myoinositol, inosine, adenosine, asparagine, aspartate, and guanosine, which have been previously reported as being depleted in metastatic PC tissue [49], indicating that activation of OR51E2 by agonists in LNCaP cells produces metabolic signatures similar to those observed in human metastatic tissues. Agonist treatment also reduced levels of intracellular urea and spermine/spermidine, in accordance with recently reported data showing reduced spermine during malignant transformation [63]. Accordingly, we also detected decreased intracellular levels of ornithine, a precursor of polyamines.

Fold change analysis of the CM revealed significantly increased glutamine (25-, 11-, and 51-fold, for 19-OH AD, AFMK, and PA, respectively), indicating that agonist-treated cells do not have an increased demand for glutamine as highly proliferating cancer cells usually do (**Figures S10B, S11B, and S12B**). Thus, these results argue for a non- or a low-proliferative phenotype. Decreased levels of docosanoic and decanoic acid and increased levels of asparagine were also prominent in the CM in

all 3 treatments (**Figure 4G**). The pathways most affected, as identified by MetaboAnalyst, were the serine, threonine, and glycine; alanine, aspartate, and glutamine; ketogenesis; arginine and proline; and beta-alanine metabolic pathways (**Figure 4F).**

Time-dependent Modulation of Cellular Proliferation

Our metabolomics results indicated reduced capacity for anabolic reactions in LNCaP cells following receptor activation, which prompted us to further analyze the effects of OR51E2 agonists on cellular proliferation. Moreover, because melatonin reduces cell proliferation, we examined whether AFMK, a melatonin metabolite, also reduces or inhibits cell proliferation [64]. LNCaP cells were stimulated with various concentrations of 19-OH AD and AFMK for 4 days and analyzed every 24 hours using an ATP viability assay. At day 4, both agonists significantly decreased the number of viable cells when compared to the control, non-stimulated cells (**Figure 5A**). This effect was dependent on cell seeding density; at higher plating densities (40% to 50%), the effect was not observed.

Cell Cycle Arrest

Next, we determined if the decrease in cell viability during agonist stimulation is attributable to increased apoptosis or cell-cycle arrest. Cells were treated with various concentrations of agonists for 3 and 7 days. Both agonists increased the fraction of cells in the G0/G1 phase and decreased the number of apoptotic cells (**Figure 5B**). Our results are in agreement with previous reports that the majority of cells with a neuroendocrine-like phenotype show signs of resistance to apoptosis [65].

Neuroendocrine Markers

To assess the effect of selected OR51E2 agonists on NEtD, we analyzed transcript levels after 3 and 12 days of stimulation of the following neuroendocrine, epithelial, and receptor genes: NSE; α-methylacyl-CoA racemase (AMACR); keratins 5, 8, and 18; voltage-gated Ca channel α1H (Cav3.2); androgen receptor (AR); and OR51E2 receptor. NSE was used to specifically identify NEtD status,

and although LNCaP (being a cell line established from lymph-node metastatasis) cells already express low levels of NSE, treatment with OR51E2 agonists significantly increase levels of the NSE transcript (**Figures 5C, 5D, and 5E**). These results correlate well with the increased intracellular level of PEP detected in the metabolomic analysis (**Figures S7B, S8B and S9B)**, since the glycolytic enzyme enolase catalyzes PEP synthesis. α-AMACR is an enzyme essential for isomerization of branched-chained fatty acids and is present at very low levels in healthy prostate and increased in PC and NE-like cells [66]. Since NE-like tumor cells express AMACR, we investigated whether activation of OR51E2 also increased AMACR levels. Indeed, AMACR levels were significantly increased after 3 and 12 days of agonist stimulation (**Figures 5C, 5D, and 5E**).

Furthermore, 19-OH AD decreased the AR transcript after 12 days, and although AFMK also showed a similar trend, it did not reach statistical significance (**Figure 5D**). Normal basal prostate epithelial cells are positive for K5, and expression of K5 is also associated with the epithelial-to-mesenchymal transition during tumor progression and metastasis [67]. K5 and K8 were not detected in the agonist-stimulated cells (data not shown). A significant decrease in K18, a luminal secretory marker, was found after 12 days of stimulation with 100 nM 19-OH AD (**Figure 5D)**. Although Ca^{+2} entry through the voltage-gated calcium channel α1H (Cav3.2) was previously reported to be involved in NEtD of LNCaP cells when cultured in steroid-free conditions, we did not detect changes in its transcript levels (data not shown) [68].

OR51E2 Knock-out Confirms NE-like Phenotype Upon Receptor Activation

To confirm receptor involvement in the agonist-mediated increase of NSE, OR51E2 was deleted using a CRISPR-Cas9 method (**Figure 5F**). We designed 3 gRNAs to target Cas9 to the OR51E2-gene and generated a lentiviral sgRNA-Cas9 vector to deliver gRNA into cells. The efficiency of each gRNA was measured, and we observed that by using sgRNA #1, OR51E2 was abrogated in 80% of cells. These OR51E2-knockout cells were exposed to 1 μM 19-OH AD for 3 days and analyzed for

the presence of specific markers (**Figures 5G and 5H**). A statistically significant decrease of NSE in OR51E2-knockout cells in comparison with control cells was observed (from 0.579 ± 0.043 in control to 0.377 ± 0.04, $P < 0.05$, n = 4 biological replicates, **Figure 5G**), confirming that increased NSE during stimulation with agonists is at least partially a receptor-mediated phenomenon (**Figures 5C and 5D)**.

DISCUSSION

As the number of ectopic olfactory receptors associated with diverse pathological states continues to increase [15,17], the implications and significance of these receptors will be greatly enhanced by receptor "deorphanization" (i.e., defining the ligands). Previously, we successfully identified novel ligands for mouse OR using a similar *in silico* approach with VLS [69]. Here, we present a highly successful approach of combining *in silico* and *in vitro* analyses to identify novel biologically relevant ligands for the human ectopic OR OR51E2. This method can be used to elucidate ligand specificities of other ectopic ORs. Once identified, these new ligands can help define the role and function of ORs in cancer and other diseases.

Among the newly discovered metabolites identified as OR51E2 agonists, several were previously reported to be associated with PC, including bradykinin, kojibiose, glycylglycine, *N*-acetylglutamic acid, and D-alanyl-D-alanine [49]. Thus, our results indicate that these metabolites are likely endogenous agonists. New agonists with known biological roles were also discovered: epitestosterone, known to be a major metabolite of androstenedione and testosterone [70]; and androstanedione (also known as 5α-androstane-3,17-dione), an intermediate in steroid synthesis [71].

In addition to these agonists, we also identified a previously under-reported metabolite of the complex steroid biosynthetic network, 19-hydroxyandrost-4-ene-3,17-dione (19-OH AD) [55,72,73]. 19-OH AD is produced by aromatase P450 (CYP19A1), which catalyzes the irreversible aromatization of the

androgens androst-4-ene-3,17-dione and testosterone and their consequent conversion to estrogens (http://www.brenda-enzymes.org/enzyme.php?ecno=1.14.14.14). We detected this testosterone metabolite in agonist-stimulated prostate cancer cells. These results demonstrate that 19-OH AD is actively produced by cancer cells when the OR51E2 receptor is activated. Thus, we demonstrate that 19-OH AD is an endogenous agonist produced by activation of OR51E2 in prostate cancer cells.

Aromatase is increased 30-fold in metastatic PC [62], and aromatase-knockout mice have a reduced incidence of PC following exposure to testosterone and estrogen, indicating that aromatase metabolites, mainly 19-OH AD and estradiol, are likely involved in prostate carcinogenesis. Results from our study demonstrate that 19-OH AD is a potent OR51E2 agonist (EC_{50}= 1.5^{-10} M) and support the notion that increased *in situ* estrogen production via 19-OH AD is an important factor in PC [61].

AFMK is a metabolite of melatonin [74]. Previous studies demonstrated that melatonin reduces proliferation of LNCaP cells, leading to NEtD, and the phenotype was not reversed by melatonin receptor antagonists, suggesting that additional receptors may be mediating this process [64,75]. Our results demonstrate that OR51E2 is a receptor for AFMK, a melatonin metabolite, and although its EC_{50} is in the μM range, much higher than reported blood concentrations (<65 pM) [76], the local tissue concentration may reach μM and mM levels as has been recently shown for keratinocytes [74]. An additional source of AFMK might be a tryptophan metabolic pathway [77]. Tumors produce high levels of tryptophan and kynurenic acid metabolites [78]. Significant amplification of tryptophan-2,3-dioxygenase (EC 1.13.11.11) TDO2, which catalyzes the oxidation of L-tryptophan to *N*-formyl-L-kynurenamine, was observed in NEPC and PC [79,80]. Thus, in more advanced stages of PC, AFMK production may be increased via this tryptophan metabolic pathway. Recently, this pathway was shown to regulate the immunosuppressive microenvironment of various tumors [81].

We also identified bradykinin as an agonist for OR51E2. In general, kinins are released during the inflammatory reaction and they are involved in angiogenesis and tumorigenesis [82,83]. Our results indicate that the activation of OR51E2 by bradykinin can also happen in the early stages of PC, when the inflammatory milieu is predominant. Prostatic secretions of PC patients have elevated levels of human kallikrein 2 [84], which produces bradykinin and thus stimulates proliferation of androgen-independent PC cells in later stages of PC [85].

The OR51E2 antagonist 13-cis RA is an endogenous component of human serum, and many of its actions can be explained by isomerization to all-trans RA and 9-cis RA, which both act via retinoid receptors. However, since 13-cis RA does not have potent gene regulatory activity, additional pathways via membrane receptors have been proposed to explain its pharmacological and anti-inflammatory actions [86]. Our results demonstrate that 13-cis RA acts via the OR51E2 receptor when expressed heterologously.

OR51E2 receptor activation by 19-OH AD, AFMK, and PA induced pronounced metabolic reprograming of LNCaP cells, with the most significant changes being decreased intracellular serine and threonine levels. Because metabolism of these amino acids includes one-carbon metabolism, which provides cofactors for biosynthetic reactions in highly proliferating cells, intracellular depletion may indicate a general decrease in anabolic reactions [87]. Furthermore, an intracellular decrease in aspartate, which is normally required for protein, purine, and pyrimidine synthesis, and an increase in the CM indicate that agonist-activated LNCaP cells are not preparing for proliferation. We also detected decreased intermediates of glycolysis (glucose-6-phosphate and fructose-6-phosphate) in activated cells. Agonist treatment decreased intracellular lactate, suggesting a slower rate of glycolysis. An intriguing result was the increased intracellular level of phosphoenolpyruvate (PEP). We also found increased NSE transcription for the glycolytic enzyme enolase, which catalyzes the formation of PEP, indicating predominance of the PEP-forming reaction.

NSE is not only a marker of neuronal differentiation and maturation characteristic of neurons and neuroendocrine cells [88], but it also has an important role in synaptogenesis [89] and is reported to be stable in the high-chloride environment characteristic of neurons, in which it reaches a concentration of 2% to 3% of the soluble protein [90]. Taken together, these results indicate that receptor activation results in a neuronal-like phenotype of LNCaP cells.

Cystine was increased in the medium after 19-OH AD and AFMK treatment (Tables S12 and S13). In healthy cells, cystine is transported into cells and reduced to cysteine, which can then be utilized for synthesis of gluthatione, a protective antioxidant. As a consequence of rapid cell growth during tumorigenesis, the production of reactive oxygen species increases, providing a proliferative signal for glutamine to enter the cell and, after deamidation, condense with cysteine to form a precursor of glutathione. However, in our experiments, the medium, but not the cells, showed increased levels of glutamine and cysteine, indicating a reduction in protective oxidative and proliferative signals in agonist-stimulated cells. The alanine/aspartate/glutamine pathway is the most affected biochemical pathway during NEtD of LNCaP cells induced by steroid-reduced medium, which corroborates our results [91] (**Figure 4F**). In cancer-associated fibroblasts, asparagine and aspartate are involved in glutamine synthesis [92], and our experiments showed decreased intracellular levels of these amino acids, suggesting increased use for intracellular synthesis of glutamine. These results might also indicate a decreased cellular influx of asparagine, since it is abundant in CM. Flux studies will be necessary to determine the exact relationship between glutamine synthesis and transport in PC cells upon receptor activation.

To explain the role of OR51E2 in PC, we propose the following model: agonist stimulation generates new cells through asymmetric division and gradually increases the subpopulation of terminally differentiated cells expressing neuroendocrine markers (see graphical abstract).

NE-like cells from PC are characterized by increased expression of NSE and AMACR and decreased expression of K18 and AR [34,93,94]. Increased expression of NSE and AMARC and decreased expression of AR and K18 following 19-OH AD and AFMK treatment demonstrate that these OR51E2 agonists induce a neuroendocrine phenotype. We confirmed that this effect is receptor-mediated, as treatment of OR51E2-knockout LNCaP cells significantly reduced the NSE and AMACR transcript levels.

Cell proliferation and differentiation have an inverse relationship, and terminal differentiation coincides with proliferation arrest and exit from the division cycle [95]. Our results demonstrate that agonist treatment during the first 3 days induces cell proliferation at a rate similar to control cells, but after 4 days the viability of these cells, as measured by ATP content, was significantly reduced. Our results also demonstrate that receptor activation results in a new subpopulation of cells that undergoes G0/G1 cell cycle arrest and has decreased DNA synthesis, which is concordant with the results from our metabolomics analysis. Cellular senescence is an irreversible growth arrest, and senescent cells actively suppress apoptosis [96]. We found that agonist treatment decreases the fraction of apoptotic cells, indicating that growth arrest likely induces cellular senescence. Future studies are needed to confirm the irreversibility of this process.

Furthermore, recent whole-exome sequencing of NEPC and CRPC showed an overlap in genomic alterations, and in both demonstrated increased amplification of the OR51E2 gene, supporting our hypothesis that this receptor contributes to the NE-phenotype of PC [79,80].

Prostatic adenocarcinomas typically contain foci of non-proliferating NE-like cells that increase in number as cancer progresses [97]. Although these cells are non-mitotic, proliferating carcinoma cells have been found in their proximity, suggesting that the non-proliferating NE-like cells likely provide paracrine stimuli for growth of the surrounding carcinoma cells [98,99]. Our results demonstrate that

activation of OR51E2 by newly-discovered PC-relevant agonists induces and/or facilitates cellular transformation, resulting in NEtD, a characteristic phenotype of CRCP. This indicates that activation of OR51E2 in PC might contribute to development of non-proliferating foci. Our data demonstrate that activation of OR51E2 results in NEtD and establish this GPCR as a novel and therapeutic target for NEPC and CRPC.

Author Contributions

Conceptualization, T.A.; Methodology, T.A., J.B., M.J.M., I.S. and S.Y.K.; Investigation, T.A., J.B., M.J.M., S.Y.K., I. S. and S. L.; Writing, T.A.; Writing, Review, and Editing, T.A., J.B., M.J.M., S.L., and H.M.; Resources, H.M.; Supervision, T.A. and H.M.

Acknowledgements

We would also like to thank Professors J. Heitman, J. Huang, M. P. Dewhirst and J. A. Chi, and Drs. C. de March and T. Zhou for their critical review on the manuscript. This study was supported by the NIDCD to H. Matsunami. The authors declare no conflict of interest.

Table 1.

NAME	HMDB	CAS	EC_{50} (potency) [M]	Max conc. used	Efficacy (relative to 1 mM PA)
D-Alanyl-d-alanine	HMDB03459	923-16-0	1.40E-05	3.16 mM	1.505
AFMK	HMDB04259	52450-38-1	1.20E-05	3.16 mM	1.483
Gamma-CEHC	HMDB01931	178167-77-6	6.40E-09	10 µM	1.286
Hydroxypyruvic acid	HMDB01352	1113-60-6	4.20E-07	316 µM	1.100
Adenosine 2',3'-c-phosphate	HMDB11616	634-01-5	2.60E-08	3.16 µM	1.025
Palmitic acid	HMDB00220	57-10-3	9.80E-09	1 mM	0.927
L-Glyceric acid	HMDB06372	28305-26-2	1.90E-09	1 mM	0.898
19-OH AD	HMDB03955	510-64-5	1.50E-10	10 µM	0.890
Androstanedione	HMDB00899	846-46-8	7.90E-10	100 µM	0.888
N-Acetylglutamic acid	HMDB01138	1188-37-0	2.30E-10	10 µM	0.879
Kojibiose	HMDB11742	NA	1.00E-06	316 µM	0.790
Bradykinin	HMDB04246	58-82-2	1.30E-09	100 µM	0.762
Imidazolone*	HMDB04363	1192-34-3	7.60E-12	10 µM	0.678
Pelargonidin	HMDB03263	134-04-3	4.20E-10	100 µM	0.621
Glycine	HMDB00123	56-40-6	5.80E-08	1 mM	0.613
2-Ketoglutaric acid	HMDB00208	328-50-7	5.50E-09	1 mM	0.594
Urea	HMDB00294	57-13-6	2.30E-08	10 mM	0.580
L-Histidinol	HMDB03431	4836-52-6	3.50E-11	100 µM	0.578
8-Hydroxyguanine	HMDB02032	5614-64-2	4.40E-13	100 nM	0.570
2-Pyrrolidinone	HMDB02039	616-45-5	1.90E-09	100 µM	0.525
Epitestosterone	HMDB00628	481-30-1	6.90E-10	10 µM	0.477
Estriol	HMDB00153	50-27-1	5.30E-05	10 µM	0.344
Tetrahydrocurcumin	HMDB05789	36062-04-1	5.70E-07	316 µM	0.284

Table 1. Potency and efficacy of 24 newly discovered OR51E2 agonists with their associated HMDB and CAS identifiers. 1,4,6-androstatriene-3,17-dione (**Figure S2**) was not included, as it is one of the previously identified compounds. Maximal concentration of each chemical used to measure efficacy in comparison to the response of 1 mM propionic acid (PA) was also indicated. *Imidazolone full name = 4-methyl-2,3-dihydro-1H-imidazol-2-one.

References

1 Dorsam, R. T. & Gutkind, J. S. G-protein-coupled receptors and cancer. *Nat Rev Cancer* **7**, 79-94, doi:10.1038/nrc2069 (2007).

2 Daaka, Y. G proteins in cancer: the prostate cancer paradigm. *Sci STKE* **2004**, re2, doi:10.1126/stke.2162004re2 (2004).

3 Tang, X. L., Wang, Y., Li, D. L., Luo, J. & Liu, M. Y. Orphan G protein-coupled receptors (GPCRs): biological functions and potential drug targets. *Acta Pharmacol Sin* **33**, 363-371, doi:10.1038/aps.2011.210 (2012).

4 Julius, D., Livelli, T. J., Jessell, T. M. & Axel, R. Ectopic expression of the serotonin 1c receptor and the triggering of malignant transformation. *Science* **244**, 1057-1062 (1989).

5 Gutkind, J. S., Novotny, E. A., Brann, M. R. & Robbins, K. C. Muscarinic acetylcholine receptor subtypes as agonist-dependent oncogenes. *Proc Natl Acad Sci U S A* **88**, 4703-4707 (1991).

6 Allen, L. F., Lefkowitz, R. J., Caron, M. G. & Cotecchia, S. G-protein-coupled receptor genes as protooncogenes: constitutively activating mutation of the alpha 1B-adrenergic receptor enhances mitogenesis and tumorigenicity. *Proc Natl Acad Sci U S A* **88**, 11354-11358 (1991).

7 Gutkind, J. S. Cell growth control by G protein-coupled receptors: from signal transduction to signal integration. *Oncogene* **17**, 1331-1342, doi:10.1038/sj.onc.1202186 (1998).

8 Gutkind, J. S. The pathways connecting G protein-coupled receptors to the nucleus through divergent mitogen-activated protein kinase cascades. *J Biol Chem* **273**, 1839-1842 (1998).

9 O'Hayre, M., Degese, M. S. & Gutkind, J. S. Novel insights into G protein and G protein-coupled receptor signaling in cancer. *Curr Opin Cell Biol* **27**, 126-135, doi:10.1016/j.ceb.2014.01.005 (2014).

10 Taub, J. S., Guo, R., Leeb-Lundberg, L. M., Madden, J. F. & Daaka, Y. Bradykinin receptor subtype 1 expression and function in prostate cancer. *Cancer Res* **63**, 2037-2041 (2003).

11 Pi, M., Parrill, A. L. & Quarles, L. D. GPRC6A mediates the non-genomic effects of steroids. *J Biol Chem* **285**, 39953-39964, doi:10.1074/jbc.M110.158063 (2010).

12 Wang, J. *et al.* The prostate-specific G-protein coupled receptors PSGR and PSGR2 are prostate cancer biomarkers that are complementary to alpha-methylacyl-CoA racemase. *The Prostate* **66**, 847-857, doi:10.1002/pros.20389 (2006).

13 Kasina, S. & Macoska, J. A. The CXCL12/CXCR4 axis promotes ligand-independent activation of the androgen receptor. *Mol Cell Endocrinol* **351**, 249-263, doi:10.1016/j.mce.2011.12.015 (2012).

14 Zhou, C. *et al.* G protein-coupled receptor GPR160 is associated with apoptosis and cell cycle arrest of prostate cancer cells. *Oncotarget* **7**, 12823-12839, doi:10.18632/oncotarget.7313 (2016).

15 Foster, S. R., Roura, E. & Thomas, W. G. Extrasensory perception: odorant and taste receptors beyond the nose and mouth. *Pharmacol Ther* **142**, 41-61, doi:10.1016/j.pharmthera.2013.11.004 (2014).

16 Zhou, T., Chien, M. S., Kaleem, S. & Matsunami, H. Single cell transcriptome analysis of mouse carotid body glomus cells. *J Physiol* **594**, 4225-4251, doi:10.1113/JP271936 (2016).

17 Abaffy, T. Human Olfactory Receptors Expression and their Role in Non-Olfactory Tissues - A mini review. *Journal of Pharmacogenomics and Pharmacoproteomics* **6**, 152, doi:DOI: 10.4172/2153-0645.1000152 (2015).

18 Spehr, M. *et al.* Identification of a testicular odorant receptor mediating human sperm chemotaxis. *Science* **299**, 2054-2058, doi:10.1126/science.1080376 (2003).

19 Pavlath, G. K. A new function for odorant receptors: MOR23 is necessary for normal tissue repair in skeletal muscle. *Cell adhesion & migration* **4**, 502-506, doi:10.4161/cam.4.4.12291 (2010).

20 Pluznick, J. L. *et al.* Olfactory receptor responding to gut microbiota-derived signals plays a role in renin secretion and blood pressure regulation. *Proceedings of the National Academy of Sciences of the United States of America* **110**, 4410-4415, doi:10.1073/pnas.1215927110 (2013).
21 Chang, A. J., Ortega, F. E., Riegler, J., Madison, D. V. & Krasnow, M. A. Oxygen regulation of breathing through an olfactory receptor activated by lactate. *Nature* **527**, 240-244, doi:10.1038/nature15721 (2015).
22 Flegel, C., Manteniotis, S., Osthold, S., Hatt, H. & Gisselmann, G. Expression profile of ectopic olfactory receptors determined by deep sequencing. *PLoS ONE* **8**, e55368, doi:10.1371/journal.pone.0055368 (2013).
23 Niimura, Y., Matsui, A. & Touhara, K. Extreme expansion of the olfactory receptor gene repertoire in African elephants and evolutionary dynamics of orthologous gene groups in 13 placental mammals. *Genome Research* **24**, 1485-1496, doi:10.1101/gr.169532.113 (2014).
24 Xu, L. L. *et al.* PSGR, a novel prostate-specific gene with homology to a G protein-coupled receptor, is overexpressed in prostate cancer. *Cancer Research* **60**, 6568-6572 (2000).
25 Xu, L. L. *et al.* Quantitative expression profile of PSGR in prostate cancer. *Prostate Cancer and Prostatic Diseases* **9**, 56-61, doi:10.1038/sj.pcan.4500836 (2006).
26 Weng, J. *et al.* Increased expression of prostate-specific G-protein-coupled receptor in human prostate intraepithelial neoplasia and prostate cancers. *Int J Cancer* **113**, 811-818, doi:10.1002/ijc.20635 (2005).
27 Xia, C., Ma, W., Wang, F., Hua, S. B. & Liu, M. Identification of a prostate-specific G-protein coupled receptor in prostate cancer. *Oncogene* **20**, 5903-5907, doi:10.1038/sj.onc.1204803 (2001).
28 Vaarala, M. H., Hirvikoski, P., Kauppila, S. & Paavonen, T. K. Identification of androgen-regulated genes in human prostate. *Mol Med Rep* **6**, 466-472, doi:10.3892/mmr.2012.956 (2012).
29 Ashida, S. *et al.* Molecular features of the transition from prostatic intraepithelial neoplasia (PIN) to prostate cancer: genome-wide gene-expression profiles of prostate cancers and PINs. *Cancer Research* **64**, 5963-5972, doi:10.1158/0008-5472.CAN-04-0020 (2004).
30 Cunha, A. C., Weigle, B., Kiessling, A., Bachmann, M. & Rieber, E. P. Tissue-specificity of prostate specific antigens: comparative analysis of transcript levels in prostate and non-prostatic tissues. *Cancer Lett* **236**, 229-238, doi:10.1016/j.canlet.2005.05.021 (2006).
31 Weigle, B. *et al.* D-GPCR: a novel putative G protein-coupled receptor overexpressed in prostate cancer and prostate. *Biochem Biophys Res Commun* **322**, 239-249, doi:10.1016/j.bbrc.2004.07.106 (2004).
32 Rodriguez, M., Siwko, S. & Liu, M. Prostate-Specific G-Protein Coupled Receptor, an Emerging Biomarker Regulating Inflammation and Prostate Cancer Invasion. *Curr Mol Med* **16**, 526-532 (2016).
33 Vashchenko, N. & Abrahamsson, P. A. Neuroendocrine differentiation in prostate cancer: implications for new treatment modalities. *Eur Urol* **47**, 147-155, doi:10.1016/j.eururo.2004.09.007 (2005).
34 Hu, C. D., Choo, R. & Huang, J. Neuroendocrine differentiation in prostate cancer: a mechanism of radioresistance and treatment failure. *Front Oncol* **5**, 90, doi:10.3389/fonc.2015.00090 (2015).
35 Komiya, A. *et al.* Neuroendocrine differentiation in the progression of prostate cancer. *Int J Urol* **16**, 37-44, doi:10.1111/j.1442-2042.2008.02175.x (2009).
36 Farach, A. *et al.* Neuronal Trans-Differentiation in Prostate Cancer Cells. *Prostate* **76**, 1312-1325, doi:10.1002/pros.23221 (2016).
37 Firestein, S. How the olfactory system makes sense of scents. *Nature* **413**, 211-218, doi:10.1038/35093026 (2001).

38 Massberg, D. *et al.* Monoterpene (-)-citronellal affects hepatocarcinoma cell signaling via an olfactory receptor. *Arch Biochem Biophys* **566**, 100-109, doi:10.1016/j.abb.2014.12.004 (2015).

39 Manteniotis, S. *et al.* Functional characterization of the ectopically expressed olfactory receptor 2AT4 in human myelogenous leukemia. *Cell Death Discov* **2**, 15070, doi:10.1038/cddiscovery.2015.70 (2016).

40 Gelis, L. *et al.* Functional Characterization of the Odorant Receptor 51E2 in Human Melanocytes. *J Biol Chem* **291**, 17772-17786, doi:10.1074/jbc.M116.734517 (2016).

41 Massberg, D. *et al.* The activation of OR51E1 causes growth suppression of human prostate cancer cells. *Oncotarget* **7**, 48231-48249, doi:10.18632/oncotarget.10197 (2016).

42 Rodriguez, M. *et al.* Prostate-specific G-protein-coupled receptor collaborates with loss of PTEN to promote prostate cancer progression. *Oncogene* **35**, 1153-1162, doi:10.1038/onc.2015.170 (2016).

43 Neuhaus, E. M. *et al.* Activation of an olfactory receptor inhibits proliferation of prostate cancer cells. *The Journal of biological chemistry* **284**, 16218-16225, doi:10.1074/jbc.M109.012096 (2009).

44 Sanz, G. *et al.* Promotion of cancer cell invasiveness and metastasis emergence caused by olfactory receptor stimulation. *PLoS ONE* **9**, e85110, doi:10.1371/journal.pone.0085110 (2014).

45 Cao, W., Li, F., Yao, J. & Yu, J. Prostate specific G protein coupled receptor is associated with prostate cancer prognosis and affects cancer cell proliferation and invasion. *BMC Cancer* **15**, 915, doi:10.1186/s12885-015-1921-6 (2015).

46 Saito, H., Chi, Q., Zhuang, H., Matsunami, H. & Mainland, J. D. Odor coding by a Mammalian receptor repertoire. *Sci Signal* **2**, ra9, doi:10.1126/scisignal.2000016 (2009).

47 Zhuang, H. & Matsunami, H. Evaluating cell-surface expression and measuring activation of mammalian odorant receptors in heterologous cells. *Nature protocols* **3**, 1402-1413, doi:10.1038/nprot.2008.120 (2008).

48 Wishart, D. S. *et al.* HMDB: the Human Metabolome Database. *Nucleic acids research* **35**, D521-526, doi:10.1093/nar/gkl923 (2007).

49 Sreekumar, A. *et al.* Metabolomic profiles delineate potential role for sarcosine in prostate cancer progression. *Nature* **457**, 910-914 (2009).

50 Key, T. J. *et al.* Plasma carotenoids, retinol, and tocopherols and the risk of prostate cancer in the European Prospective Investigation into Cancer and Nutrition study. *The American journal of clinical nutrition* **86**, 672-681 (2007).

51 Nyman, D. W. *et al.* Selenium and selenomethionine levels in prostate cancer patients. *Cancer detection and prevention* **28**, 8-16, doi:10.1016/j.cdp.2003.11.002 (2004).

52 Sekihara, H. 19-Hydroxyandrostenedione: evidence for a new class of sodium-retaining and hypertensinogenic steroids. *Endocrinology* **113**, 1141-1148, doi:10.1210/endo-113-3-1141 (1983).

53 Sekihara, H. 19-Hydroxyandrostenedione: a potent hypertensinogenic steroid in man. *J Steroid Biochem* **19**, 353-358 (1983).

54 Sekihara, H. Evidence that 19-hydroxyandrostenedione is secreted by the adrenal cortex and is under the control of ACTH and the renin-angiotensin system in man. *Biochem Biophys Res Commun* **105**, 610-614 (1982).

55 Tosha, T. *et al.* Raman evidence for specific substrate-induced structural changes in the heme pocket of human cytochrome P450 aromatase during the three consecutive oxygen activation steps. *Biochemistry* **45**, 5631-5640, doi:10.1021/bi060094a (2006).

56 Raeside, J. I., Renaud, R. L., Friendship, R. M. & Khalil, M. W. Secretion of 19-hydroxyandrostenedione and 19-hydroxytestosterone by porcine Leydig cells in vitro and in vivo. *J Endocrinol* **137**, 281-289 (1993).

57 Norton, B. I., Miyairi, S. & Fishman, J. 19-Hydroxylation of androgens by rat granulosa cells. *Endocrinology* **122**, 1047-1052, doi:10.1210/endo-122-3-1047 (1988).

58 McDunn, J. E. *et al.* Metabolomic signatures of aggressive prostate cancer. *Prostate* **73**, 1547-1560, doi:10.1002/pros.22704 (2013).

59 Carruba, G. Estrogen and prostate cancer: an eclipsed truth in an androgen-dominated scenario. *J Cell Biochem* **102**, 899-911, doi:10.1002/jcb.21529 (2007).

60 Jackson, E. K. The 2',3'-cAMP-adenosine pathway. *Am J Physiol Renal Physiol* **301**, F1160-1167, doi:10.1152/ajprenal.00450.2011 (2011).

61 Ricke, W. A. *et al.* Prostatic hormonal carcinogenesis is mediated by in situ estrogen production and estrogen receptor alpha signaling. *FASEB J* **22**, 1512-1520, doi:10.1096/fj.07-9526com (2008).

62 Montgomery, R. B. *et al.* Maintenance of intratumoral androgens in metastatic prostate cancer: a mechanism for castration-resistant tumor growth. *Cancer Res* **68**, 4447-4454, doi:10.1158/0008-5472.CAN-08-0249 (2008).

63 Shukla-Dave, A. *et al.* Ornithine Decarboxylase Is Sufficient for Prostate Tumorigenesis via Androgen Receptor Signaling. *Am J Pathol* **186**, 3131-3145, doi:10.1016/j.ajpath.2016.08.021 (2016).

64 Sainz, R. M. *et al.* Melatonin reduces prostate cancer cell growth leading to neuroendocrine differentiation via a receptor and PKA independent mechanism. *Prostate* **63**, 29-43, doi:10.1002/pros.20155 (2005).

65 Fixemer, T., Remberger, K. & Bonkhoff, H. Apoptosis resistance of neuroendocrine phenotypes in prostatic adenocarcinoma. *Prostate* **53**, 118-123, doi:10.1002/pros.10133 (2002).

66 Huang, J. *et al.* Immunohistochemical characterization of neuroendocrine cells in prostate cancer. *Prostate* **66**, 1399-1406, doi:10.1002/pros.20434 (2006).

67 Verhagen, A. P., Aalders, T. W., Ramaekers, F. C., Debruyne, F. M. & Schalken, J. A. Differential expression of keratins in the basal and luminal compartments of rat prostatic epithelium during degeneration and regeneration. *Prostate* **13**, 25-38 (1988).

68 Mariot, P., Vanoverberghe, K., Lalevee, N., Rossier, M. F. & Prevarskaya, N. Overexpression of an alpha 1H (Cav3.2) T-type calcium channel during neuroendocrine differentiation of human prostate cancer cells. *J Biol Chem* **277**, 10824-10833, doi:10.1074/jbc.M108754200 (2002).

69 Bavan, S., Sherman, B., Luetje, C. W. & Abaffy, T. Discovery of novel ligands for mouse olfactory receptor MOR42-3 using an in silico screening approach and in vitro validation. *PLoS One* **9**, e92064, doi:10.1371/journal.pone.0092064 (2014).

70 Starka, L. Epitestosterone. *J Steroid Biochem Mol Biol* **87**, 27-34 (2003).

71 Chang, K. H., Ercole, C. E. & Sharifi, N. Androgen metabolism in prostate cancer: from molecular mechanisms to clinical consequences. *Br J Cancer* **111**, 1249-1254, doi:10.1038/bjc.2014.268 (2014).

72 Harkonen, P. *et al.* Sex hormone metabolism in prostate cancer cells during transition to an androgen-independent state. *J Clin Endocrinol Metab* **88**, 705-712, doi:10.1210/jc.2002-020236 (2003).

73 Fishman, J. & Goto, J. Mechanism of estrogen biosynthesis. Participation of multiple enzyme sites in placental aromatase hydroxylations. *J Biol Chem* **256**, 4466-4471 (1981).

74 Tan, D. X., Manchester, L. C., Terron, M. P., Flores, L. J. & Reiter, R. J. One molecule, many derivatives: a never-ending interaction of melatonin with reactive oxygen and nitrogen species? *J Pineal Res* **42**, 28-42, doi:10.1111/j.1600-079X.2006.00407.x (2007).

75 Lupowitz, Z. & Zisapel, N. Hormonal interactions in human prostate tumor LNCaP cells. *J Steroid Biochem Mol Biol* **68**, 83-88 (1999).

76 Harthe, C. *et al.* Radioimmunoassay of N-acetyl-N-formyl-5-methoxykynuramine (AFMK): a melatonin oxidative metabolite. *Life Sci* **73**, 1587-1597 (2003).

77 Ximenes, V. F., Catalani, L. H. & Campa, A. Oxidation of melatonin and tryptophan by an HRP cycle involving compound III. *Biochem Biophys Res Commun* **287**, 130-134, doi:10.1006/bbrc.2001.5557 (2001).
78 Opitz, C. A. *et al.* An endogenous tumour-promoting ligand of the human aryl hydrocarbon receptor. *Nature* **478**, 197-203, doi:10.1038/nature10491 (2011).
79 Beltran, H. *et al.* Divergent clonal evolution of castration-resistant neuroendocrine prostate cancer. *Nat Med* **22**, 298-305, doi:10.1038/nm.4045 (2016).
80 Cerami, E. *et al.* The cBio cancer genomics portal: an open platform for exploring multidimensional cancer genomics data. *Cancer Discov* **2**, 401-404, doi:10.1158/2159-8290.CD-12-0095 (2012).
81 Platten, M., von Knebel Doeberitz, N., Oezen, I., Wick, W. & Ochs, K. Cancer Immunotherapy by Targeting IDO1/TDO and Their Downstream Effectors. *Front Immunol* **5**, 673, doi:10.3389/fimmu.2014.00673 (2014).
82 Naidu, N., Botha, J. H. & Naidoo, S. B1 but not B2 bradykinin receptor agonists promote DU145 prostate cancer cell proliferation and migration. *Afr Health Sci* **14**, 657-662, doi:10.4314/ahs.v14i3.22 (2014).
83 Bhoola, K. D., Figueroa, C. D. & Worthy, K. Bioregulation of kinins: kallikreins, kininogens, and kininases. *Pharmacol Rev* **44**, 1-80 (1992).
84 Charlesworth, M. C., Young, C. Y., Miller, V. M. & Tindall, D. J. Kininogenase activity of prostate-derived human glandular kallikrein (hK2) purified from seminal fluid. *J Androl* **20**, 220-229 (1999).
85 Raj, G. V., Barki-Harrington, L., Kue, P. F. & Daaka, Y. Guanosine phosphate binding protein coupled receptors in prostate cancer: a review. *J Urol* **167**, 1458-1463 (2002).
86 Blaner, W. S. Cellular metabolism and actions of 13-cis-retinoic acid. *J Am Acad Dermatol* **45**, S129-135, doi:10.1067/mjd.2001.113714 (2001).
87 Kalhan, S. C. & Hanson, R. W. Resurgence of serine: an often neglected but indispensable amino Acid. *J Biol Chem* **287**, 19786-19791, doi:10.1074/jbc.R112.357194 (2012).
88 Isgro, M. A., Bottoni, P. & Scatena, R. Neuron-Specific Enolase as a Biomarker: Biochemical and Clinical Aspects. *Adv Exp Med Biol* **867**, 125-143, doi:10.1007/978-94-017-7215-0_9 (2015).
89 Whitehead, M. C., Marangos, P. J., Connolly, S. M. & Morest, D. K. Synapse formation is related to the onset of neuron-specific enolase immunoreactivity in the avian auditory and vestibular systems. *Dev Neurosci* **5**, 298-307 (1982).
90 Marangos, P. J. & Schmechel, D. E. Neuron specific enolase, a clinically useful marker for neurons and neuroendocrine cells. *Annu Rev Neurosci* **10**, 269-295, doi:10.1146/annurev.ne.10.030187.001413 (1987).
91 Cerasuolo, M. *et al.* Neuroendocrine Transdifferentiation in Human Prostate Cancer Cells: An Integrated Approach. *Cancer Res* **75**, 2975-2986, doi:10.1158/0008-5472.CAN-14-3830 (2015).
92 Yang, L. *et al.* Targeting Stromal Glutamine Synthetase in Tumors Disrupts Tumor Microenvironment-Regulated Cancer Cell Growth. *Cell Metab* **24**, 685-700, doi:10.1016/j.cmet.2016.10.011 (2016).
93 Yuan, T. C., Veeramani, S. & Lin, M. F. Neuroendocrine-like prostate cancer cells: neuroendocrine transdifferentiation of prostate adenocarcinoma cells. *Endocr Relat Cancer* **14**, 531-547, doi:10.1677/ERC-07-0061 (2007).
94 Yin, B. *et al.* Downregulation of cytokeratin 18 is associated with paclitaxelresistance and tumor aggressiveness in prostate cancer. *Int J Oncol* **48**, 1730-1736, doi:10.3892/ijo.2016.3396 (2016).
95 Ruijtenberg, S. & van den Heuvel, S. Coordinating cell proliferation and differentiation: Antagonism between cell cycle regulators and cell type-specific gene expression. *Cell Cycle* **15**, 196-212, doi:10.1080/15384101.2015.1120925 (2016).

96 Childs, B. G., Baker, D. J., Kirkland, J. L., Campisi, J. & van Deursen, J. M. Senescence and apoptosis: dueling or complementary cell fates? *EMBO Rep* **15**, 1139-1153, doi:10.15252/embr.201439245 (2014).

97 di Sant'Agnese, P. A. Neuroendocrine differentiation in human prostatic carcinoma. *Hum Pathol* **23**, 287-296 (1992).

98 Terry, S. & Beltran, H. The many faces of neuroendocrine differentiation in prostate cancer progression. *Front Oncol* **4**, 60, doi:10.3389/fonc.2014.00060 (2014).

99 Cox, M. E., Deeble, P. D., Lakhani, S. & Parsons, S. J. Acquisition of neuroendocrine characteristics by prostate tumor cells is reversible: implications for prostate cancer progression. *Cancer Res* **59**, 3821-3830 (1999).

100 Katoh, K., Misawa, K., Kuma, K. & Miyata, T. MAFFT: a novel method for rapid multiple sequence alignment based on fast Fourier transform. *Nucleic acids research* **30**, 3059-3066 (2002).

101 Ring, A. M. *et al.* Adrenaline-activated structure of beta2-adrenoceptor stabilized by an engineered nanobody. *Nature* **502**, 575-579, doi:10.1038/nature12572 (2013).

102 Sali, A. & Blundell, T. L. Comparative protein modelling by satisfaction of spatial restraints. *Journal of molecular biology* **234**, 779-815, doi:10.1006/jmbi.1993.1626 (1993).

103 Shen, M. Y. & Sali, A. Statistical potential for assessment and prediction of protein structures. *Protein science : a publication of the Protein Society* **15**, 2507-2524, doi:10.1110/ps.062416606 (2006).

104 Abagyan, R., Totrov, M. & Kuznetsov, D. ICM-A new Method for Protein Modeling and Design: applications to Docking and Structure Prediction from the Distorted Native Conformation. *Journal of Computational Chemistry* **15**, 488-506 (1994).

105 Abaffy, T., Malhotra, A. & Luetje, C. W. The molecular basis for ligand specificity in a mouse olfactory receptor - A network of functionally important residues. *J Biol Chem* **282**, 1216-1224, doi:DOI 10.1074/jbc.M609355200 (2007).

106 Neves, M. A. C., Totrov, M. & Abagyan, R. Docking and scoring with ICM: the benchmarking results and strategies for improvement. *Journal of Computer-Aided Molecular Design* **26**, 675-686, doi:DOI 10.1007/s10822-012-9547-0 (2012).

107 Rege, J. *et al.* Liquid chromatography-tandem mass spectrometry analysis of human adrenal vein 19-carbon steroids before and after ACTH stimulation. *J Clin Endocrinol Metab* **98**, 1182-1188, doi:10.1210/jc.2012-2912 (2013).

108 Chen, J., Meng, C. K., Narayan, S. B., Luan, W. & Bennett, M. J. The use of Deconvolution Reporting Software and backflush improves the speed and accuracy of data processing for urinary organic acid analysis. *Clin Chim Acta* **405**, 53-59, doi:10.1016/j.cca.2009.04.005 (2009).

109 Halket, J. M. *et al.* Deconvolution gas chromatography/mass spectrometry of urinary organic acids--potential for pattern recognition and automated identification of metabolic disorders. *Rapid Commun Mass Spectrom* **13**, 279-284, doi:10.1002/(SICI)1097-0231(19990228)13:4<279::AID-RCM478>3.0.CO;2-I (1999).

110 He, J. *et al.* MuRF2 regulates PPARgamma1 activity to protect against diabetic cardiomyopathy and enhance weight gain induced by a high fat diet. *Cardiovasc Diabetol* **14**, 97, doi:10.1186/s12933-015-0252-x (2015).

111 McNulty, N. P. *et al.* The impact of a consortium of fermented milk strains on the gut microbiome of gnotobiotic mice and monozygotic twins. *Sci Transl Med* **3**, 106ra106, doi:10.1126/scitranslmed.3002701 (2011).

112 Quintana, M. T. *et al.* Cardiomyocyte-Specific Human Bcl2-Associated Anthanogene 3 P209L Expression Induces Mitochondrial Fragmentation, Bcl2-Associated Anthanogene 3 Haploinsufficiency, and Activates p38 Signaling. *Am J Pathol* **186**, 1989-2007, doi:10.1016/j.ajpath.2016.03.017 (2016).

113 Kind, T. *et al.* FiehnLib: mass spectral and retention index libraries for metabolomics based on quadrupole and time-of-flight gas chromatography/mass spectrometry. *Anal Chem* **81**, 10038-10048, doi:10.1021/ac9019522 (2009).
114 Xia, J. & Wishart, D. S. Using MetaboAnalyst 3.0 for Comprehensive Metabolomics Data Analysis. *Curr Protoc Bioinformatics* **55**, 14 10 11-14 10 91, doi:10.1002/cpbi.11 (2016).
115 Goeman, J. J., van de Geer, S. A., de Kort, F. & van Houwelingen, H. C. A global test for groups of genes: testing association with a clinical outcome. *Bioinformatics* **20**, 93-99 (2004).

MATERIAL AND METHODS

Homology Modeling

Amino acid sequences of bovine rhodopsin, the human adrenergic beta-2-receptor β 2AR, the mouse olfactory receptor MOR42-3, and the human olfactory receptor OR51E2, were initially aligned using a MAFFT program [100]. Our model was built based on the crystal structure of β2AR (4LDO; [101]). We used BioEdit Sequence Alignment Editor (http://www.mbio.ncsu.edu/BioEdit/bioedit.html) to manually remove gaps in the β2AR and OR51E2 sequences and re-align Cys178 in OR51E2 (EC2) with Cys191 from the β2AR sequence (**Figure S1**). β2AR has a disulfide bond between the conserved Cys106 residue at the N-terminal end of TM3 and Cys191 from EC2. Thus, to introduce a disulfide bond we re-aligned equivalent cysteines in OR51E2 (Cys96-Cys178). In addition, the most conserved residues were also aligned (Asp41, Leu54, Cys96, Leu114, Asp120, Arg121, Tyr122, Pro128, Pro159, Tyr217, Asp287, Pro288, Ile290, and Tyr290). We used Modeller v.9.14 to create homology models [102] **(**http://salilab.org/modeller/), and 20 homology models were made using an automodel script with the default optimization and refinement. Each model was assessed using a DOPE score [103]. The best model, which had a DOPE score of -37275, was chosen for further analysis. This .pdb file was imported into ICM Software (MolSoft v.3.8, LLC, La Jolla, CA) [104], and the protein structure was analyzed using Ramchandran Plot Analysis. Residues that were out of place (Glu90, Arg222, His180, Leu81, and Lys294) were optimized. The model was transformed into an ICM object and subjected to regularization and minimization using MMFF Cartesian minimization (300 steps). The

minimized model was imported into Modeller and again evaluated to calculate DOPE score (new DOPE = -38897). This final, minimized model was used for docking and VLS in the ICM program.

Virtual Library Screening

The library used for VLS was selected from the HMDB (www.HMDB.ca) and consisted of metabolites detected in human blood, tissue, urine, and saliva. VLS was performed with the ICM software as described previously [69]. Briefly, the potential energy maps of the receptor were made in a box with a 0.5-Å grid and a size of 53 x 50 x 45 Å. The initial position of the ligand was set within the center of this box, which extends to the receptor interior (above the center positions of Ser107 and Ala108, which are equivalent positions to Ile112 and Val113 in MOR42-3 that are known to be part of the ligand binding pocket [105]). The docking stimulation was set to 1 and the maximal number of conformations to 10. The remainder of the docking parameters were set at the default values. The VLS result lists ligand-metabolite pairs according to their scores, and lower scores indicate ligands that are more likely to bind to the receptor. Binding of the ligand to the receptor is described using Score and mfScore functions. The Score function is based on a *theoretical calculation* of receptor-ligand binding energy:

$$\Delta G = \Delta E_{IntFF} + T\Delta S_{Tor} + \alpha 1 \Delta E_{HBond} + \alpha 2 \Delta E_{HBDesol} + \alpha 3 \Delta E_{SolEl} + \alpha 4 \Delta E_{HPhob} + \alpha 5 Q_{Size}$$

The mfScore function is a *knowledge-based* potential derived from the frequencies of occurrence of various atom pairs within the experimental ligand/receptor complex structures deposited in the Protein Data Bank (PDB) [106]. It represents a measure of statistical probability of interaction between the ligand and receptor. Our previous results indicate that both scoring functions were equally successful in predicting ligands [69]. The top 50 hits from each scoring list are presented in **Tables S1 and S2**.

Cell Culture

Prostate cancer LNCaP-FGC cells derived from lymph node metastatic site (passage 30-32) were obtained from the American Type Culture Collection (ATCC). Cells were maintained at 37°C in RPMI-1640 medium (Sigma R8758) enriched with 0.5% glucose (45%, Sigma G8769), 1% 1 M HEPES (Gibco-Thermo 15630), 1% 100 mM Na-pyruvate (Gibco-Thermo 11360), 10% FBS (HyClone, SH30071.03), 100 U/mL penicillin, and 0.1 mg/mL streptomycin. At 4 to 5 days after seeding, cells were 70% to 80% confluent and the stimulus was applied at the indicated concentration for the indicated time. The medium was replaced every fourth day.

Luciferase Assay

Briefly, the OR51E2 plasmid was transfected into HANA3A cells along with a CREB-dependent luciferase (firefly) and a constitutively active luciferase (*Renilla*) [46]. Upon ligand binding, an increase in cAMP drives the expression of firefly luciferase and increases the signal. To control for variation in cell number and transfection efficiency, the luciferase signal was normalized to the activity of the *Renilla* luciferase in the same cells. All stock solutions of chemicals were prepared either in dimethylsulfoxide (DMSO) or ethanol. Final dilutions were made in M10d medium. M10d is MEM medium enriched with 5% dialyzed FBS serum, which is devoid of small molecular weight compounds (<10,000 Da), since OR51E2-transfected cells gave a high luciferase signal in the CD293 medium (Gibco 11913-019, supplemented with 30 μM $CuCl_2$ and 2 μM L-glutamine) even in the absence of chemical stimulation and when compared to the basal activity of the control OR2W1 receptor-expressing cells (data not shown). All compounds that did not show agonist activity in M10d were later diluted in CD293 medium and tested for antagonist activity. The rest of the protocol was performed as previously published [46]. Cells were exposed to candidate ligands for 3.5 hours at various concentrations. For each compound that showed a response >2 SD of the baseline response (no chemical applied), the EC_{50} or IC_{50} was determined from a sigmoid dose-response curve using a

Graph-Pad Prism (Graph-Pad Prism Software, San Diego, USA). Data were fitted to the equation: Y = Bottom + (Top-Bottom)/(1+10^((LogIC50-X) *HillSlope)).

19-OH AD measurements using LC/MS

LNCaP cells were first grown in T-75 flasks until just fully confluent. Cells were then split into 6 T-25 flasks Cells were exposed to 250 μM AFMK, or to the medium only, for 3 days. We used phenol-red free RPMI 1640 with 10% CD-serum (Hyclone, SH30068) or RPMI 1640 with 10% FBS, as described in cell culture protocol. After 3 days, medium was collected and frozen at -80^{o}C until LC/MS measurements.

In 2 mL polypropylene vial, 800 μL of cell media sample was vigorously mixed with 1 mL of ethyl acetate, centrifuged, and 900 μL of the organic (top) layer evaporated under a stream of nitrogen at room temperature. To the dried residue, 20 μL of the following reagent for picolinoyl ester derivatization was added: 40 mg of picolinic acid, 20 mg of 2-methyl-6-nitrobenzoic anhydride (MNBA), 10 mg of 4-dimethyl-laminopyridine, 1 mL acetonitrile, and 20 μL trimethylamine. After 20 min incubation at 50^{o}C, 30 μL of 0.1% formic acid in water was added and 25 μL sample injected into the LC-MS/MS system (slightly modified from [107]. LC conditions (Shimadzu 20A series HPLC): Agilent Eclipse PLUS, C18, 50 x 4.6 mm, 1.8 μm particle size column; mobile phases A/B: 0.1% formic acid in water/acetonitrile; elution gradient: 0-1min 20-90%B, 1-1.5min 90%B, 1.5-1.7min 90-20%B; run-time: 5min. Mass spectrometer conditions (AB/Sciex API5500 QTrap): after optimization of the electrospray and quadrupoles parameters by infusion of 100 ng/mL 19-OHAD at 10 μL/min rate, 408.2/267.2 MS/MS transition was used for quantification.

Metabolomics GC-MS Analysis

LNCaP cells were first grown in T-75 flasks until just fully confluent. Cells were then split into 6 T-25 flasks and exposed to agonists the following day: 250 μM AFMK, 100 nM 19-OH AD, or 1 mM

propionic acid (PA), with 6 biological replicates in each group. After agonist treatment for 3 days, CM was removed and banked at -80°C, and the cells were rinsed with 10 mL ice-cold PBS. Next, 3 mL of ice-cold 0.9% NaCl were added, and cells were scraped off of the plates and transferred to 5-mL tubes that were previously cleaned with acetonitrile. Each flask was rinsed with an additional 2 mL of ice-cold 0.9% NaCl, and the cell suspensions were transferred to the 5-mL tubes and centrifuged at 1000 rpm for 5 min at 4°C. Supernatant was removed, and 200 μL of ice-cold dH_20 with 0.6% formic acid were added to the cell pellets. Then, 20 μL of resuspended cell pellets were separated for protein measurements (Qubit Protein Assay kit, Cat. # Q33211, Thermo Fisher Scientific), and 180 μL of acetonitrile were added to the remaining pellet. Prepared cell lysates were maintained at -80°C until metabolomics analysis.

For exploratory, non-targeted metabolomics via gas chromatography/mass spectrometry (GC/MS), metabolites were extracted from cell lysates with methanol, methoximated in dry pyridine, and then silylated with *N*-methyl-*N*-(trimethylsilyl) trifluoroacetamide. Samples were analyzed on a 6890N GC connected to a 5975 MS (Agilent Technologies, Santa Clara, CA) equipped with 2 wall-coated open-tubular (WCOT) GC columns connected in series (Agilent part 122-5512, DB5MS, 15 m in length, 0.25 mm in diameter, with an 0.25-μm luminal film) separated by a microfluidic flow splitter to enable hot back-flushing at the end of each run [108]. Data were acquired by scanning from *m/z* 600 to 50 as the oven ramped from 70°C to 325°C. Data were deconvoluted using AMDIS software [109]. Metabolites were identified using our retention time-referenced spectral library [110-112], which is based in part on that of Kind *et al.* [113]. Reported data are $\log_2$ transforms of the areas of deconvoluted peaks.

Data were normalized to the protein content in each sample. MetaboAnalyst 3.0 was used for statistical analysis [114]. Briefly, peak intensity data were presented in columns and $\log_2$-normalized. We used unpaired analysis, and data were auto-scaled (mean-centered and divided by the standard

deviation of each variable). For pathway analysis, we used a Globaltest pathway-enrichment analysis algorithm [115] in MetaboAnalyst 3.0.

RT-PCR Analysis

LNCaP cells were grown in T-75 flasks until fully confluent. A split ratio of 1:6 was used to subculture the cells in T-25 flasks for 24 to 48 hours before stimulation. Stimulation with agonists lasted 3 or 12 days. Medium was changed every 4 days in the 12-day experiment. Total RNA was extracted using Trizol reagent (Invitrogen) and cleaned using the RNeasy kit (Qiagen) following the manufacturer's protocol. Integrity of total RNA was confirmed by agarose gel electrophoresis. cDNA was generated by reverse transcription using SuperScript II Reverse Transcriptase (Invitrogen). Primers for the following genes were designed with the Primer 3.0 program: OR51E2, NSE-neuron-specific enolase, AMACR-α-methylacyl-CoA racemase, α1H T-type calcium channel (Cav3.2), AR-androgen receptor, GAPDH, keratin 5, keratin 8, and keratin 18 (**Table S3**). PCR amplification was performed with HotStart Taq Polymerase (Qiagen) using the following protocol: 95°C for 15 min followed by 30 cycles at the following times and temperatures: 95°C for 15 s, 55°C for 15 s, and 72°C for 30 s. Final annealing was done at 72°C for 5 min. Expression levels of the test genes were normalized to GAPDH.

Cell Proliferation Assay

Cells were plated in five 96-well plates (100 μL cell suspension per well) and after overnight attachment when cells were 15% to 20% confluent, cells were stimulated with increasing concentrations of selected agonists. Cell growth and viability was estimated each day for the next 4 days by using Cell Titer-Glo Luminescent Cell Viability Assay (Promega, Cat. No. G7570) according to the manufacturer's instructions.

Cell Cycle Analysis

LNCaP cells were plated in 100-mm Petri dishes. After overnight attachment, when cells were 40% to 50% confluent, cells were stimulated once with 100 nM 19-OH AD and 250 μM AFMK for the next 4 days. Cells incubated in the regular RPMI-1640 medium served as controls. After treatment, cells were trypsinized with 0.05% trypsin-EDTA (Gibco) and fixed with 70% ethanol in PBS for 15 min at 4°C. Fixed cells were washed and incubated with 50 μg/μL RNase A and 20 μg/μL propidium iodide and subjected to cell cycle analysis using a Becton Dickinson FACSCalibur cytometer. Data were analyzed with BD CellQuest software. Experiments were performed 3 times in triplicate (3 biological and 3 technical replicates).

LNCaP OR51E2 Knockout Cell Lines

To generate CRISPR/Cas9-mediated knockout LNCaP cells, we cloned sgRNAs targeting exon 2 of OR51E2 into LentiCRISPR.v2 (Addgene #52961) for coexpression of sgRNA with *Streptococcus pyogenes* Cas9. We prepared lentiviral particles for each sgRNA vector by cotransfecting HEK293T cells with the LentiCRISPR vectors psPAX2 and pMD2.g using TransIT-LT1 (Mirus). LNCaP cells were transduced with this virus at a multiplicity of infection (MOI) of <1 in the presence of 8 μg/ml polybrene. At 24 hours post-infection, cells were selected with 2 μg/mL puromycin for 72 hours and then expanded for verification of gene editing and experimental analysis. Cells were harvested for genomic DNA and PCR amplification of the OR51E2 locus for the Surveyor Assay (Integrated DNA Technologies) 1 week after infection. Additionally, for stable cells harboring OR51E2 sgRNA #1, PCR products were cloned into a TOPO-TA cloning vector (ThermoFisher Scientific) and Sanger sequenced to assess the rate of mutation.

Sequences:

sgRNA #1:CGTGGTCTTCATCGTAAGGA

sgRNA #2:AGGCCTCAAAGCTAATCTCT

sgRNA #3:CATTGAATCCACCATCCTGC

OR51E2 forward: ACGAAGGTATGGACCAGTAGGA

OR51E2 reverse:AAGACCATATACCACATTGGGC

Quantification and Statistical Analysis

All results are expressed as means ± SEM. Computations assumed that all groups were samples from populations with the same scatter. The investigators involved in this study were not completely blinded during sample collection or data analysis. Significance was determined by (multiple) two-tailed unpaired t-test using Prism 7 software. A P value of 0.05 was considered significant.

Reagent and Resource Table

REAGENT or RESOURCE	SOURCE	IDENTIFIER
Chemicals, Peptides, and Recombinant Proteins		
Alpha-n-phenylacetyl-l-glutamine	Sigma-Aldrich	CH6371381881
Estriol	Sigma-Aldrich	285803
Epitestosterone	Sigma-Aldrich	E-058
19-hydroxyandrost-4-ene-3,17-dione	Sigma-Aldrich	779717
Testosterone	Steraloids	A6950-000
Palmitic acid	Sigma-Aldrich	P0500
Stearoylethanolamide	Sigma-Aldrich	S8439
Androstenedione	Sigma-Aldrich	A-075
Androstanedione (5alpha androstan 3,17, dione)	Sigma-Aldrich	A-8255
Palmitoylethanolamide	Sigma-Aldrich	P0359
Pentadecanoic acid	Sigma-Aldrich	91446
Arachidonic acid	Sigma-Aldrich	10931
13-cis-retinoic acid	Sigma-Aldrich	R3255
D-alanyl-D-alanine	Sigma-Aldrich	A0912
Glycyl-glycine	Sigma-Aldrich	G0674
1,4,6 androstatrien-3,17-dione	Steraloids	A4100-000
6-dehydrotestosterone	Steraloids	A0450-000
Beta-ionone	Sigma-Aldrich	8.18619 EMD MILLIPORE
Kojibiose	Sigma-Aldrich	K4769
Urea	Sigma-Aldrich	1.08488
N1-acetylspermidine	Bocsci	14278-49-0
Glyceraldehyde	Sigma-Aldrich	G5001
N8-acetylspermidine	Sigma-Aldrich	A3658
4-acetamidobutanoic acid	Sigma-Aldrich	S458368
AFMK acetyl-n-formyl-5-methoxykynurenamine	Sigma-Aldrich	A2355
Asymmetric dimethylaariginine	Sigma-Aldrich	COM964465970
Ureidopropionic acid	Sigma-Aldrich	94295
Ureidoisobutyric acid	Sigma-Aldrich	74005
N-acetylputrescine	Sigma-Aldrich	A8784
Pelargonidin	Sigma-Aldrich	P1659

Lipoamide	Sigma-Aldrich	T5875
Histamine	Sigma-Aldrich	53290
Hydroxyacetone	Sigma-Aldrich	138185
Hydroxypyruvic acid	Sigma-Aldrich	6372
Imidazolone	Enamine	BBV-44213154
2-pyrrolidinone	Sigma-Aldrich	240338 ALDRICH
Oxoglutaric acid	Sigma-Aldrich	K1750
L-glyceric acid	Sigma-Aldrich	51738
Normetanephrine	IsoSciences	ISO-S10416UNL1.0
Glycine	Sigma-Aldrich	50046
Adenosine 2',3'-cyclic phosphate	Santa Cruz	sc-207262
Gamma-cehc	Cayman-Biomol	CAY-89630
Tetrahydrocurcumin	Santa Cruz	sc-391609
D-maltose	Santa Cruz	sc-215288
Orotidine	Santa Cruz	sc-222103
Acetaminophen glucuronide	BOC Sciences	16110-10-4
12,13-epome	Santa Cruz	sc-220590A
N-acetylvanilalanine	AKOS	AKOS013465745
Nandrolone	Sigma-Aldrich	N7252
N-acetylglutamic acid	Santa Cruz	16110-10-4
L-histidinol	AKOS	AKOS006348033
Bradykinin	Sigma-Aldrich	05-23-0500
Homo-l-arginine	Santa Cruz	sc-479071
Putreanine	AKOS	AKOS005216076
2,3-diaminopropionic acid	AKOS	AKOS006230079
Akos006230079	MolPort	MolPort-002-054-631
Critical commercial assays		
Quibit protein assay kit	Thermo Fisher Scientific	Cat# Q33211
Rneasy Kit	Qiagen	Cat# 74104
Luciferase dual-glo assay kit	Promega	Cat#E2920
Cell titer-glo luminescent cell viability assay	Promega	Cat# G7570
Surveyor assay	Integrated DNA Technologies	Cat#706021
Experimental Models: Cell Lines		
LNCaP-FGC cell line	ATCC	ATCC-CRL1740
Oligonucleotides (https://www.idtdna.com/site)		
Primer: OR51E2Fw Forward: ATATTTGCAAGCTCGGCCCT		
Primer: OR51E2Rv Reverse: GCGTTCCGTCCTTACGATGA		
Primer: ENO2Fw Forward: TCGCTTTGCCGGACATAACT		
Primer: ENO2Rv Reverse: GTGCGGAACCCCAATGAGTA		
Primer: AMACRFw Forward: AAGACGAAGGCAGAGTGGTG		
Primer: AMACRRv Reverse: ATCTCTTCGCGGCTGAATCC		
Primer: CaV3Fw Forward: ATGCCGACTGCCACATAGAG		
Primer: CaV3Rv Reverse: ACCACATGCGGGATCTTCTC		
Primer: ARFw Forward: CCGGAAGCTGAAGAAACTTGG		
Primer: ARRv Reverse: CCACGTGTACAAGCTGTCTCT		
Primer: GAPDH-Fw Forward: CATCACTGCCACCCAGAAGA		
Primer: GAPDH-Rv Reverse: GTCAAAGGTGGAGGAGTGGG		
Primer: KRT5-Fw Forward: GAGATCGCCACTTACCGCAA		
Primer: KRT5-Rv Reverse: GTAGCTTCCACTGCTACCTCC		
Primer: KRT8-Fw Forward: GAATGAATGGGGTGAGCTGG		
Primer: KRT8-Rv Reverse: CTCTGGTTGACCGTAACTGC		
Primer: KRT18-Fw Forward: TCCTTTCTCTCTCCCCGGAC		
Primer: KRT18-Rv Reverse: CGTTCTGGATGCCTCCCATT		

Software and Algorithms		
MAFFT program	Katoh et al., 2002	https://mafft.cbrc.jp/alignment/software/
BioEdit Sequence Alignment Editor		http://www.mbio.ncsu.edu/BioEdit/bioedit.html
Modeller v. 9.14	Sali and Blundell, 1993	http://salilab.org/modeller/
ICM MolSoft v.3.8	Abagyan et al., 1994	www.molsoft.com
HMDB	Wishart D. S., 2007	www.HMDB.ca
Graph-Pad Prism	Graph-Pad Prism Software, San Diego	https://www.graphpad.com
AMDIS	Halket et al., 1999	www.amdis.net

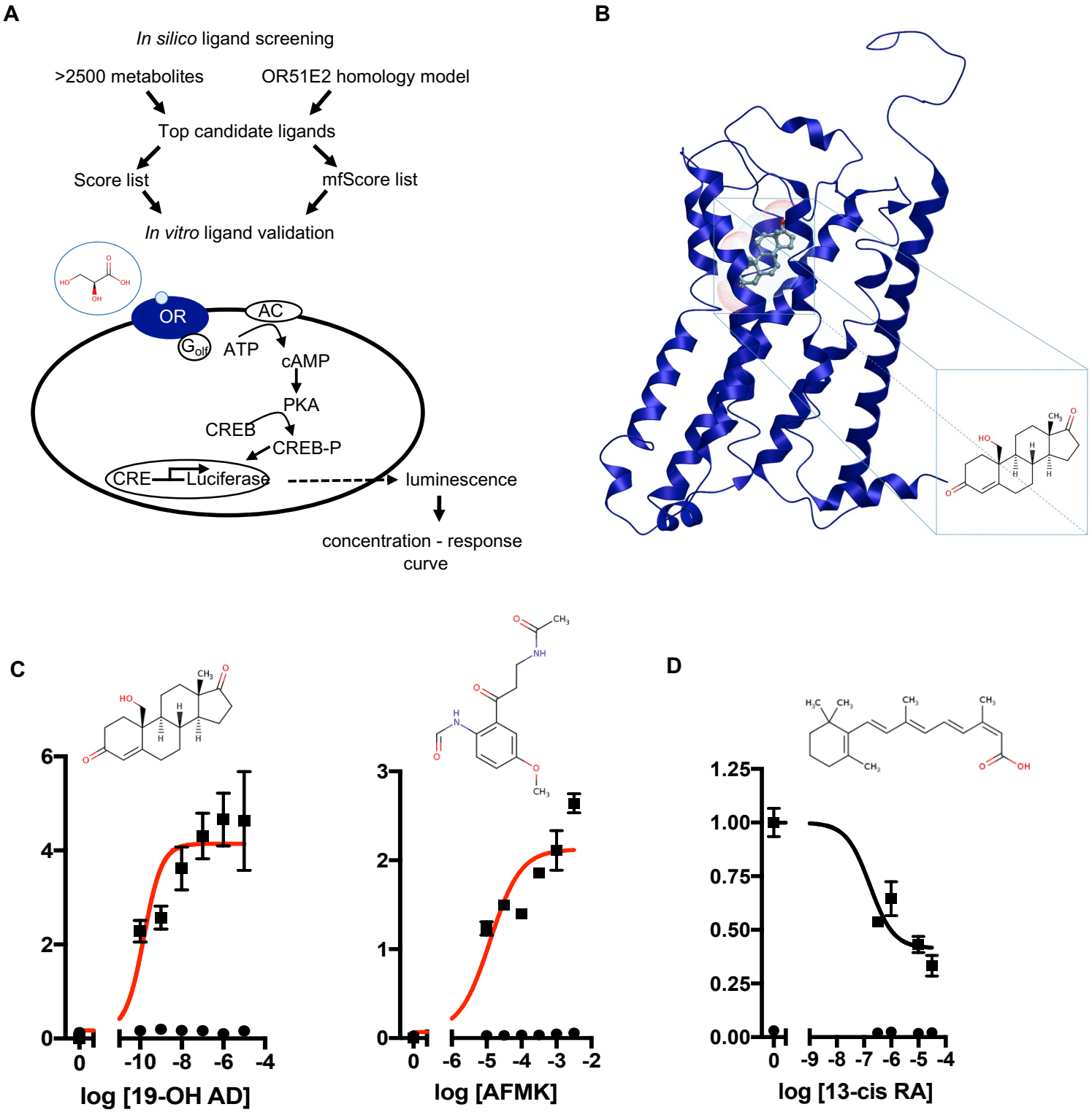

Figure 1. Discovery of novel endogenous metabolite-ligands for OR51E2. A. Study design. **B.** Homology model of OR51E2 with 19-hydroxyandrost-4-ene-3,17-dione (19-OH AD) docked into the receptor pocket. **C.** Concentration - response curves for 19-OH AD and AFMK (red) and their structures. **D.** Concentration - response curve for antagonist 13-cis retinoic acid (13-cis RA). N=3, mean ± SEM.

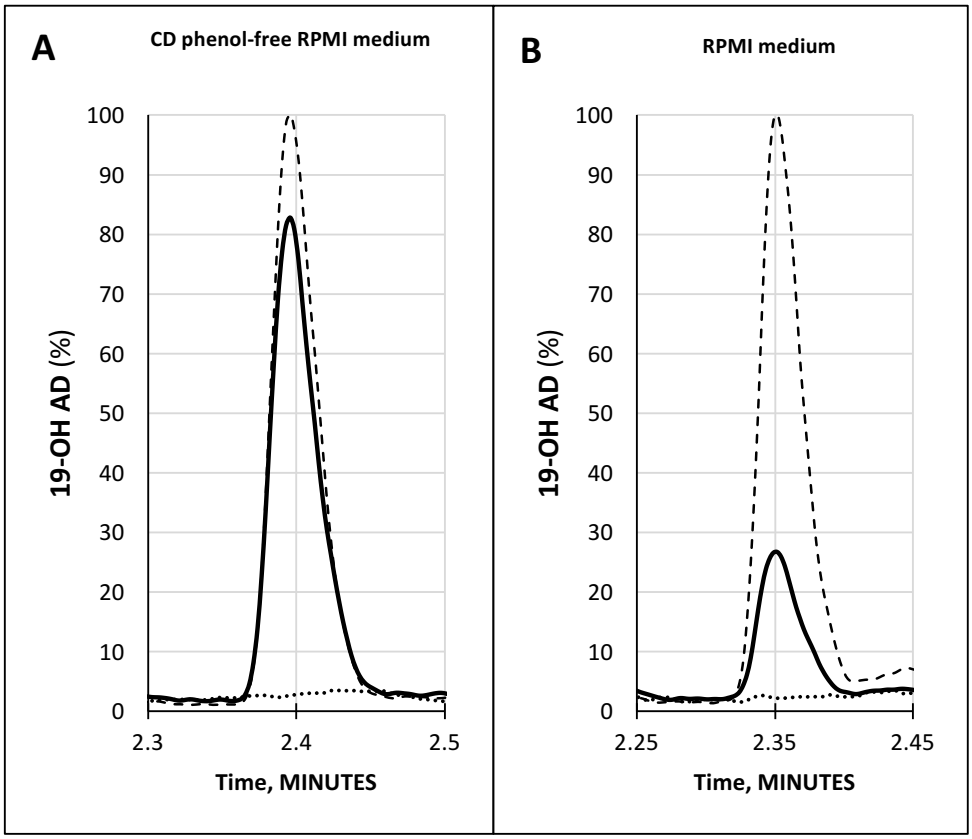

Figure 2. Quantification of 19-OH AD by LC-MS/MS in the medium from AFMK-stimulated LNCaP cells. (**A**) CD phenol-free RPMI medium with 250 μM AFMK (solid line), 1 ng/mL of 19-OH AD- standard spike (dashed line); estimated concentration of 19-OH AD is 0.83 ng/mL medium. (**B**) RPMI medium + 250 μM AFMK (solid line), 1 ng/mL 19-OH AD of standard spike (dashed line); estimated concentration of 19-OH AD is 0.27 ng/mL. Dotted lines at the bottom in A and B are media only, with no AFMK. Curves are normalized to 1ng/mL 19-OH AD.

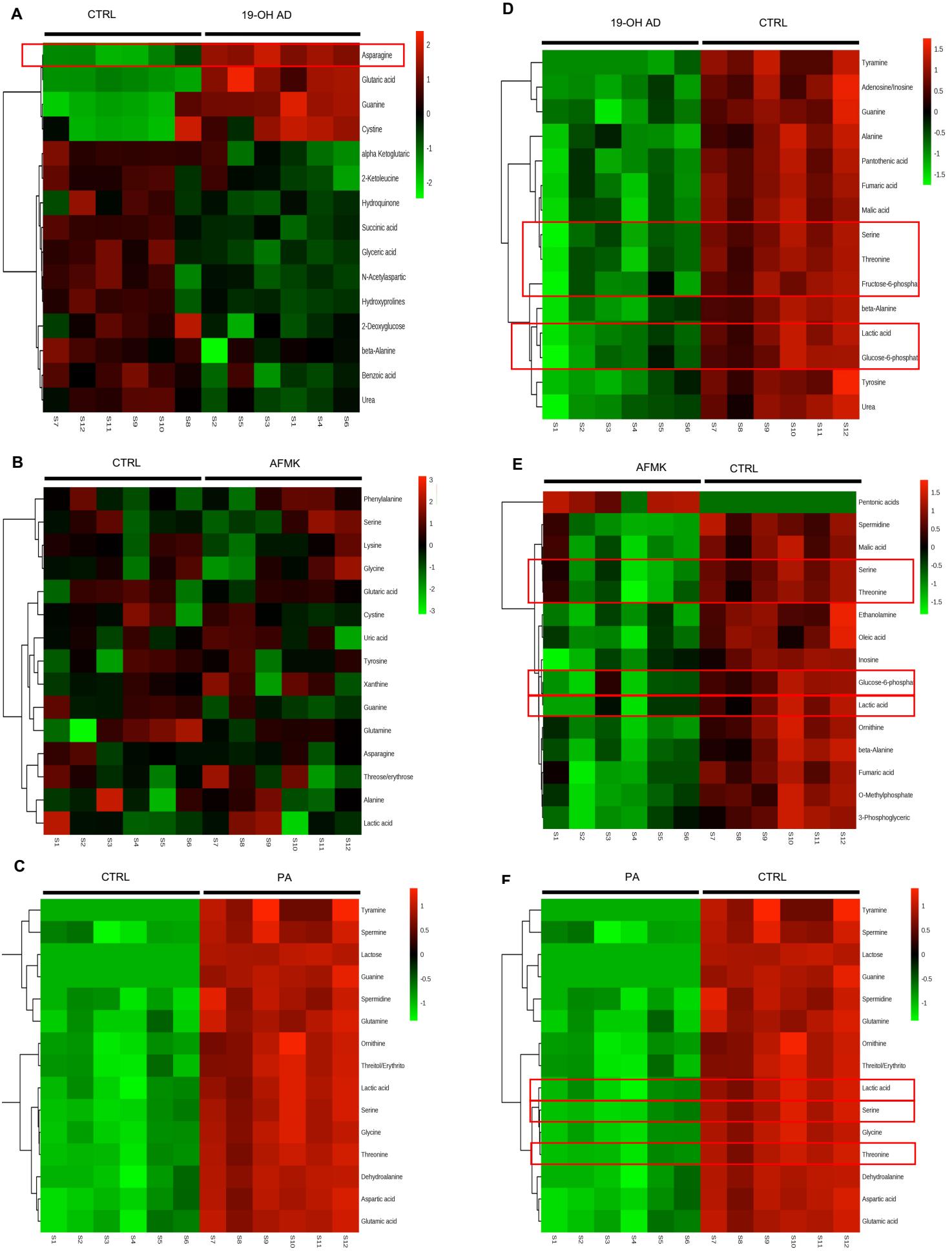

Figure 3. Agonist treatment of LNCaP cells results in robust metabolomic signatures. The top 15 extracellular metabolites identified after stimulation with **A.** 19-OH AD, **B.** AFMK, and **C.** PA. The top 15 intracellular metabolites identified after stimulation with **D.** 19-OH AD, **E.** AFMK, and **F.** PA. Heatmaps are based on the Pearson correlation analysis (Ward) and indicate annotated metabolites identified by t-test *(P* < 0.05, FDR <0.1, n = 6). Columns correspond to the samples treated with agonists (S1-6) and control (S7-12), and rows correspond to annotated metabolites.

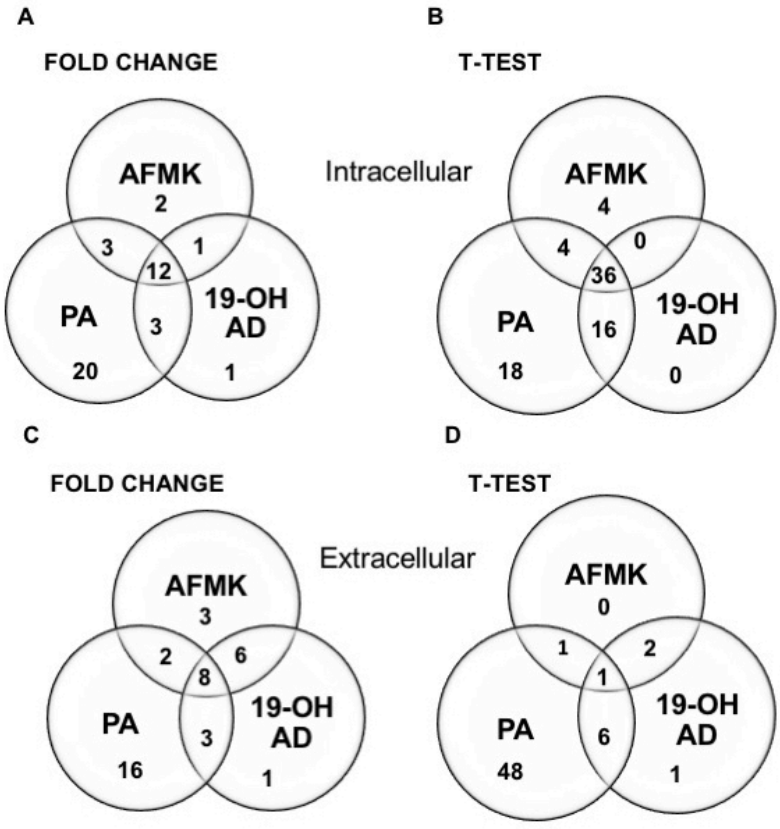

E

Decreased intracellular metabolites in agonist-treated cells	
3-Phosphoglyceric acid	Hydroxyprolines
Adenine	Hypoxanthine
Adenosine	Inosine
Alanine	Lactic acid
Aldo/Keto pentose-5-phosphate	Lactose
Arachidonic acid	Lysine
Asparagine	Malic acid
Aspartic acid	O-Methylphosphate
Beta-alanine	Oleic acid
Dihydroxyacetone phosphate	Ornithine
Ethanolamine	Pantothenic acid
Fructose-6-phosphate	Phosphoric acid
Fumaric acid	Serine
Gluconic acid	Spermidine
Glucose-6-phosphate	Succinic acid
Glycine	Threonine
Guanine	Tyramine
Guanosine	Urea

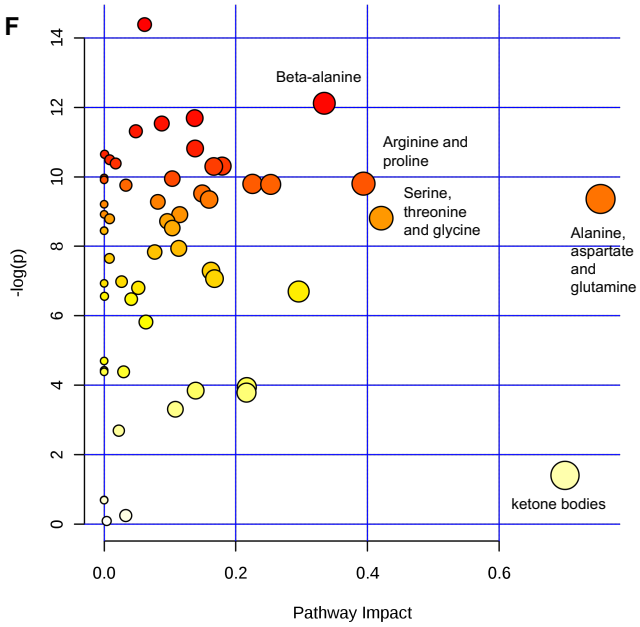

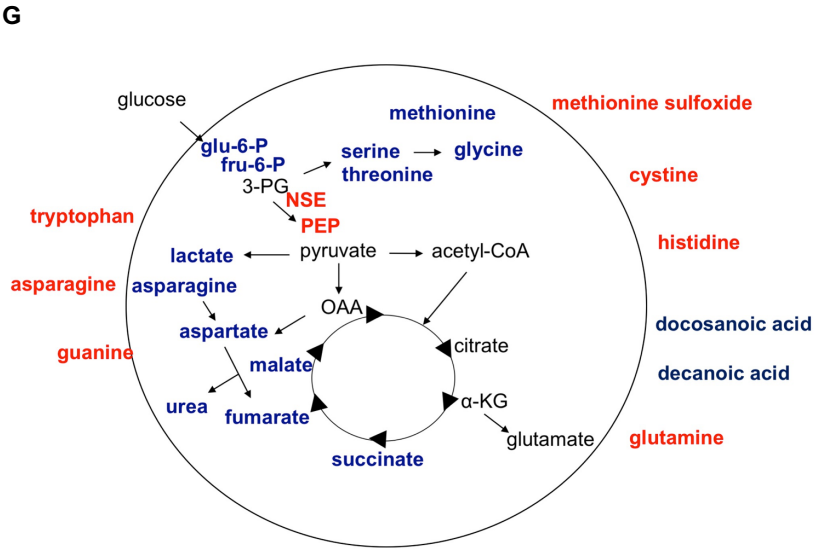

Figure 4. Most pronounced metabolic changes induced by activation of OR51E2 with selected agonists. Venn diagrams show the set of annotated intracellular metabolites differentially expressed by (**A**) fold change and (**B**) t-test analysis, and the set of extracellular metabolites identified by (**C**) fold change and (**D**) t-test. **E.** In total, 36 annotated intracellular metabolites significantly decreased in all 3 treatments (see **3B**). **F.** Pathway analysis. The most pronounced pathways in 19-OH AD-treated cells. Pathways are displayed as circles, and the color and size of each circle is based on its *P* value and pathway impact value, respectively. The top-right area indicate the most significant changes in metabolites. **G.** Schematic representation of cellular metabolites. Significantly increased metabolites are in bold red, and significantly decreased are in bold blue (PEP - phosphoenol pyruvate, OAA - oxalacetate, 3PG – 3-phosphoglycerate, α-KG - α-ketoglutarate). Increased NSE (neuron-specific enolase) catalyzes the formation of PEP and is also indicated in red.

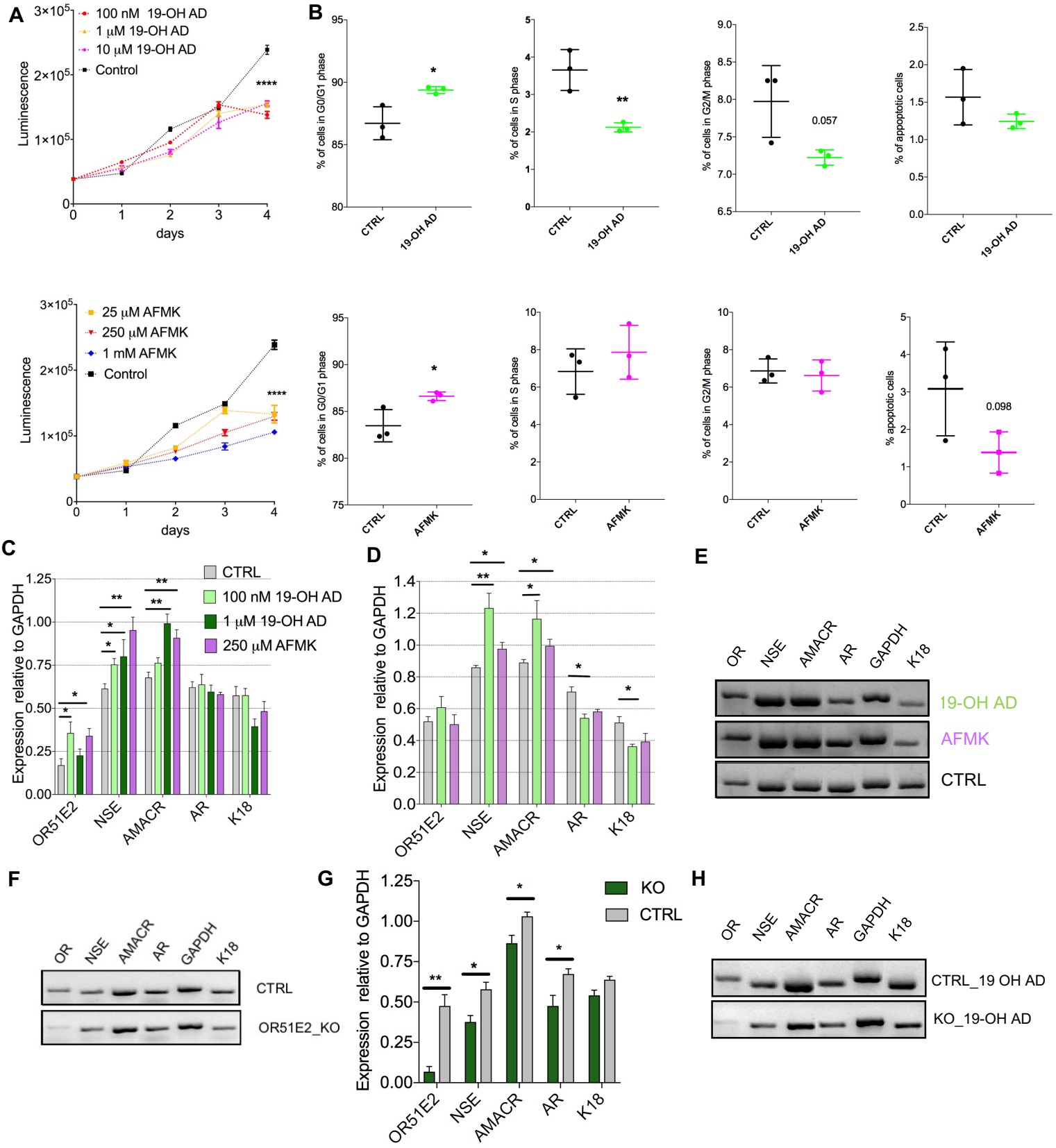

Figure 5. Activation of OR51E2 receptor by selected agonists induces a neuroendocrine phenotype. A. Cell viability assay at various indicated concentrations of 19-OH AD and AFMK. Cell viability correlates with luminescence signal. Statistical significance at day 4 with 100 nM 19-OH AD and 250 μM AFMK is ****P <0.0001. **B.** Cell cycle analysis after incubation with 100 nM 19-OH AD and 250 μM AFMK for 7 and 3 days, respectively. **C.** Transcript levels of markers after agonist stimulation for 3 days; N = 3 to 6, unpaired t-test, **P <0.01. *P <0.05 **D**. Transcript levels of makers after stimulation with agonists for 12 days, N= 3 to 6, unpaired t-test, **P <0.01. *P <0.05 **E.** Representative gel image of data presented in D. **F.** Markers in the OR51E2-knockout (KO) and control cells (CTRL). **G.** Transcript levels of markers relative to GAPDH after 3 days stimulation with 1 μM 19-OH AD in OR51E2-KO LNCaP cells. N=4, mean ± SEM. **P <0.01. *P <0.05.